

department of electrical engineering



(NASA-CR-125685) A THIN POLYMER INSULATOR
FOR JOSEPHSON TUNNELING APPLICATIONS
Semiannual Report, Sep. 1971 - Feb. 1972
C. W. Wilmsen, et al (Colorado State Univ.)
Feb. 1972 30 p
N72-19802
Unclas 15136
CSCL 20L G3/26

Colorado State University
Department of Electrical Engineering
Fort Collins, Colorado 80521

A THIN POLYMER INSULATOR FOR JOSEPHSON TUNNELING APPLICATIONS

Semi-Annual Report

February 1972

C. W. Wilmsen

J. C. Robertson



NASA Grant No. NGR 06-002-094

Office of Research Grants and Contracts
Office of Space Science and Applications
National Aeronautics and Space Administration
Washington, D.C. 20546

Reproduced by
NATIONAL TECHNICAL
INFORMATION SERVICE
U.S. Department of Commerce
Springfield VA 22151

Colorado State University
Department of Electrical Engineering
Fort Collins, Colorado 80521

A THIN POLYMER INSULATOR FOR JOSEPHSON
TUNNELING APPLICATIONS

Semi-Annual Report

February 1972

C. W. Wilmsen

J. C. Robertson

NASA Grant No. NGR 06-002-094
Office of Research Grants and Contracts
Office of Space Science and Applications
National Aeronautics and Space Administration
Washington, D. C. 20546

I. Introduction

This report outlines the progress made during the last six months towards forming thin organic layers on superconductors and how these layers effect the transition temperature. The work during this time has been primarily directed towards 1) synthesis of the organics, 2) deposition of organics, and 3) setting up to make transition temperature measurements.

The greatest effort during this period was placed on the synthesis of the organics. As a result most of the synthesis procedures are now perfected. Our efforts now turn to experimenting with deposition of the organics and measurement of the transition temperature.

Those contributing to the research during this report period are:

Dr. Carl Wilmsen - Associate Professor,
Electrical Engineering

Dr. Jerry Robertson - Assistant Professor,
Chemistry

Mr. Don Stuehm - Research Assistant,
Electrical Engineering

Mr. Paul Hammer - Lab Assistant,
Chemistry

Mr. Bruce Martin - Lab Assistant,
Chemistry

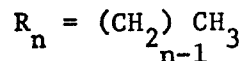
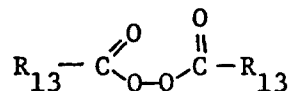
II. Synthesis of Organics

Two major efforts were required; one, to synthesize organic which will chemisorb on the superconductors and the other, to label the organics with Carbon-14 in order to investigate the deposition process.

a) Carbon 14 labeling

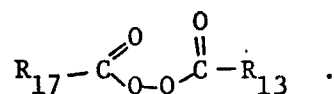
Presently we are using two organics:

Myristyl Peroxide



and

Steryl Peroxide



Synthesis of these molecules is not difficult, but to label the molecules with a radioactive carbon using very small quantities is a delicate process. Small quantities must be used since the C-14 is quite expensive and it is not convenient to work with a large radiation source. The synthesis procedure was first worked out with nonradioactive compounds. Only the myristyl peroxide will be discussed here.

The first attempt at synthesis was with silyl esters but the yield was very low.

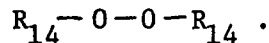
The second approach converted malonic acid to malonyl chloride and then to diethyl malonate and then finally to myristic peroxide. Because of the small quantities used, the malonyl chloride synthesis was not adequately complete.

The third method was successful and is outlined in more detail. The method basically converts malonic acid to diethyl malonate by dissolving malonic acid and ethanol in toluene with sulfuric acid as a catalysis. With some work, an almost 100% yield was obtained. This step is followed

by subjecting the diethyl malonate to butanol in the presence of sodium metal. This converts the diethyl ester to a sodium salt which when stirred with dodecyl bromide, goes to dodecyl diethyl malonate and sodium bromide. The large diester is then treated with potassium hydroxide which converts the diester to a diacid salt. Hydrochloric acid is then used to convert the potassium salt to the diacid. The diacid is then heated to about 180°C allowing α , β , Keto elimination to occur leaving the labeled myristic peroxide in the form of an oil layer. The literature calls for fractional distillation of the myristic peroxide, but because of the small amount of material present this has not worked. Acid-base extractions as well as regular extractions have also failed. However, cooling the oil until myristic peroxide precipitates out allows the trapping of the myristic peroxide.

b) Synthesis of Tetradecyl Peroxide

A third and more promising organic for monolayer deposition is tetradecyl peroxide,



This molecule has never been made before with the carbon chain larger than 7. However, we have been able to synthesize the molecule and here we outline the synthesis procedure.

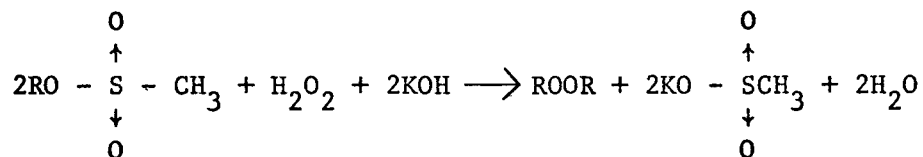
Tetradecyl peroxide has been synthesized by the reaction of alkyl methanesulfonates in aqueous methanol solvent in the presence of potassium hydroxide at room temperature with 30% hydrogen peroxide.

The alkyl methanesulfonate was readily prepared in good yield by the action of methanesulfonyl chloride on myristic alcohol in the presence of pyridine.



This was a fairly quick intermediate to prepare and it had a fairly high yield $\approx 80\%$. The problem was now to convert this intermediate to tetradecyl peroxide.

The literature indicated that alkyl methanesulfonate could be employed successfully in the alkylation of hydrogen peroxide to give primary and secondary dialkyl peroxides in satisfactory yields when two moles of alkyl methanesulfonate were used for each mole of hydrogen peroxide.

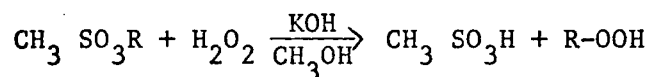


According to this equation, the dialkyl peroxide was the predominant reaction product.

If one considers the competing side reactions, basic hydrolysis of the alkyl methanesulfonate, decomposition of the hydrogen peroxide and the intermediate alkyl hydroperoxide itself, it is a wonder that yields as high as 45 to 65% as reported in literature tables has been obtained.

Thus far, the products we have isolated using this method, have not been consistent with literature tables as to melting points or I.R. Spectra.

In some cases it is thought that the product was the intermediate hydroperoxide



perhaps being caused by an excess of hydrogen peroxide being used.

In other cases, perhaps the potassium hydroxide decomposed the hydrogen peroxide in which case the methanesulfonate remained unreacted. In one trial it is sure this happened, because I.R. Spectra was identical on sulfonate and what was thought would be peroxide. A second method yields the tetradecyl peroxide in reasonable quantities. The details are given here.

A mixture of .1 mole of the methanesulfonate, .05 mole of 30% H_2O_2 and 30 ml of methanol was cooled to 0° . .1 mole of 50% aqueous KOH was added over a period of a few minutes with stirring, and the mixture was allowed to come slowly to room temperature.

Since it had been determined that 30% H_2O_2 slowly decomposed in the presence of base in methanol solution of this concentration and temperature, a second addition of .025 mole of 30% H_2O_2 was made after approximately five hours.

The reaction mixture was then allowed to stir for an additional 22 hours. Then the reaction mixture was worked up by adding water, extracting the aqueous solution with several 10 ml portions of hexane, and washing the hexane layer with 5 ml of 5% KOH to remove any hydroperoxide. Then washing the hexane layer with distilled water until the washings were neutral, and drying the hexane layer over anhydrous sodium sulfate distillation of the residue to give the peroxide.

III. Deposition of the Organics

In previous tests we have used an ultra-high vacuum system with a background pressure of $\approx 10^{-9}$ torr. However, using this vacuum system required several days and considerable effort to complete an experiment. Therefore, for the time being, we will use a clean diffusion pump system which has a good liquid nitrogen trap. We are also experimenting with different ways of introducing the organic into the vacuum. The deposition of organics will be of primary concern during the next two-three months.

IV. Transition Temperature Movement

In order to make accurate T_c measurements we have purchased a mini cryostat and matching helium Dewar. This set up is quick and easy to use with a low helium consumption rate. We will use standard four lead measurement techniques. We expect to start this phase of the work in two-three months.

V. Josephson Junction Analysis

The Josephson junction characteristics can be used to study very thin insulators. As a result of our study of the effects of shorts and pinholes in the insulator of the Josephson junction, we have come to some important conclusions concerning the Josephson junction quantum interferometer. This information is included in two papers, which have been submitted for publication. These papers are included as appendixes.

APPENDIX I

Multiple Junction Asymmetric Feed

Quantum Interometers

By

D. L. Stuehm and C. W. Wilmsen

Applied Physics Letters

MULTIPLE JUNCTION ASYMMETRIC FEED
QUANTUM INTERFEROMETERS*

D. L. Stuehm and C. W. Wilmsen
Electrical Engineering Department
Colorado State University
Fort Collins, Colorado 80521

ABSTRACT

The three junction asymmetric feed Josephson junction quantum interferometer has been analyzed and shown to have increased magnetic field sensitivity and amplitude deviation over the two junction interferometer. The critical current at zero applied field is shown to be less than the critical current at zero flux in the interference loop.

The Josephson junction quantum interferometer¹ is used as a magnetic field sensing device capable of measuring either the absolute value of or the variation of a magnetic field. To measure variations of a magnetic field the interferometer is operated on the steepest portion of the interference pattern. Recently Clarke and Paterson^{2,3} have demonstrated that driving the two junction interferometer with an asymmetric current feed produces an asymmetric interference pattern which increases one slope of the interference pattern. This increased slope increases the interferometers sensitivity to changes in magnetic fields.

We have developed a numerical technique for analyzing Josephson junction quantum interferometers and report here analysis of the two and three Josephson junction asymmetrical current feed interferometers. The numerical results show that the three junction interferometer not only has increased magnetic field sensitivity but also has a larger amplitude variation (dynamic range) compared to the two junction interferometer. The numerical results also indicate that zero applied magnetic field is not coincident with the peak value of critical current making the asymmetrical feed interferometer less attractive for absolute magnetic field measurements.

The geometry of an asymmetrical current feed three junction interferometer is shown in Fig. 1. The magnetic field due to the current per unit width, I , for this configuration always subtracts from the applied magnetic field (H_e) which is into the plane of the paper. The current density through the junctions is related to the superconducting pair phase $\phi(z)$ by the Josephson equation

$$J(z) = j_1 \sin \phi(z) \quad (1)$$

The gradient of the pair phase is related to the local magnetic field by

$$\frac{d\phi(z)}{dz} = \frac{2ed_1}{\hbar c} H(z) \quad (2)$$

where d_1 is twice the London penetration depth plus the thickness of

the barrier. Combining eqns. 1 and 2 with Maxwell's equation

$$\frac{dH(z)}{dz} = \frac{4\pi}{c} J(z) \quad (3)$$

produces the differential equation

$$\frac{d^2\phi(z)}{dz^2} = \frac{1}{\lambda_J^2} \sin \phi(z) \quad (4)$$

which relates the pair phase difference across the junction to the junctions spacial dimensions ($\lambda_J^2 = \hbar c^2 / 8\pi e d_1 j_1$). If $\phi(z)$ is known in the junction then $H(z)$ in the junction can be computed from eq. 2. For an interference loop length much larger than its height (d_2), a uniform magnetic field in the interference loop can be assumed along with continuity of H field at the junction interference loop boundary. The pair phase across the interference loop is then

$$\phi(z) = \phi(L_1) + \frac{d_2}{d_1} \frac{d\phi(L_1)}{dz} (z-L_1) \quad L_1 \leq z \leq L_2 \quad (5)$$

The initial conditions for solving eq. 4 at the next junction are also obtained from eq. 5. This technique can be continued for any number of junctions. One initial condition for the first junction comes from applying Ampere's law and eq. 2 to the boundaries around the outer perimeter of the interferometer.

$$\frac{d\phi(0)}{dz} = \frac{2ed_1}{\hbar c} \left(H_e - \frac{4\pi}{c} I \right) \quad (6)$$

The other initial condition, $\phi(0)$, is found by interating between 0 and 2π until the boundary condition

$$\frac{d\phi(L)}{dz} = \frac{2ed_1}{\hbar c} H_e \quad (7)$$

is satisfied for a given current per unit width, I , and applied magnetic field H_e . If I is chosen to be larger than the critical current, no solution to the differential equations will exist. Also I can be computed by integrating eq. 1 over all the junctions and comparing the computed I with the I used in the initial condition. These equations, which were solved numerically, take into consideration the applied magnetic field and the magnetic field due to the currents flowing in the superconducting links. Also, the spacial variations of the pair phase in the junctions due to the junction current and applied magnetic field are considered in the equations.

Figure 2 illustrates the numerically calculated interference patterns for both the two and three junction interometers. For the two junction interferometer it can be seen that:

1. Increasing the junction length with constant loop area (curves a and b) increases the maximum pattern slope but also reduces the percentage amplitude change of the oscillation.
2. Increasing the loop area with constant junction length (curves a and c) decreases the amplitude but increases the slope.

Thus both methods for increasing the pattern slope, decreases the percentage amplitude change of the interference pattern. A decrease in percentage amplitude variation makes the interference pattern more difficult to detect. One can increase the current level through the interferometer

by increasing the width which does not affect the characteristics of the interference pattern. These results are consistent with the work of Clarke and Paterson.^{3,4} It should also be pointed out that as the junction size becomes very small, e.g., a point contact device, the asymmetry of the interference pattern becomes negligibly small.

In Fig. 2 the interference pattern of the three junction interferometer can be compared with three different two junction interferometers. In each case important parameters of the two and three junction devices are equal.

These are:

curves a and d - equal total loop area and equal junction length.

curves b and d - equal total loop area and equal total junction length.

curves c and d - equal junction length and equal loop area.

For all three of these cases, the three junction interferometer has considerably greater pattern slope and amplitude. In fact the slope of the three junction device is up to seven times as great, with the amplitude about twice that of the two junction devices.

Note that the peak current of the three junction interferometer is less than the two junction peak (curves b and d), even though the total junction lengths are equal and the junction lengths are much less than λ_J . This can be explained as follows: the highest peak for the two junction device occurs when there is zero flux in the interference loop. However, zero flux cannot occur simultaneously in both loops of the three junction junction device since the H field has a non-zero slope through the middle junction. Thus, if the flux is zero in one loop, the flux in the other loop must be non-zero and the total current cannot reach the peak of the two junction interferometer.

It is also seen that the applied magnetic field required to produce zero loop flux, must be increased when the junction lengths are increased (a to b or c to b). Maximum current flows through the interferometer at zero loop flux because the magnetic fields in the junctions are minimum at that point. This leads to the technologically more important conclusion that for asymmetric feed interferometers, zero applied magnetic field does not coincide with the maximum current through the interferometer.⁵

Absolute magnetic field measurements are therefore not conveniently made with the asymmetric feed interferometer.

REFERENCES

* Supported in part by NASA.

1. R. C. Jaklevic, J. Lambe, J. E. Mercereau and A. H. Silver, Phys. Rev. 140, A1628 (1965).
2. J. Clarke and J. L. Paterson, Bull. Am. Phys. Soc. 16, 399 (1971).
3. J. Clarke and J. L. Paterson, Appl. Phys. Letters, 19, 469 (1971).
4. J. Clarke and J. L. Paterson, University of California Radiation Lab Report UCRL-20579.
5. Zero applied magnetic field coincides with the maximum current through the interferometer for the symmetrical feed device.

FIGURES

Fig. 1 The geometry of the three junction asymmetric current feed interferometer. The shaded areas are the Josephson junctions. H_e is the applied magnetic field directed into the paper. I is the current per unit width through the device. The center junction is removed for a two junction interferometer.

Fig. 2 Interference patterns for four interferometers. The three solid lines are for two junction interferometers. The dashed line is for a three junction interferometer. The interferometer dimensions are:

$$a) L_1 = .1\lambda_J, L-L_4 = .1\lambda_J, (L_4-L_1)d_2 = 40\lambda_J d_1;$$

$$b) L_1 = .15\lambda_J, L-L_4 = .15\lambda_J, (L_4-L_1)d_2 = 40\lambda_J d_1;$$

$$c) L_1 = .1\lambda_J, L-L_4 = .1\lambda_J, (L_4-L_1)d_2 = 20\lambda_J d_1;$$

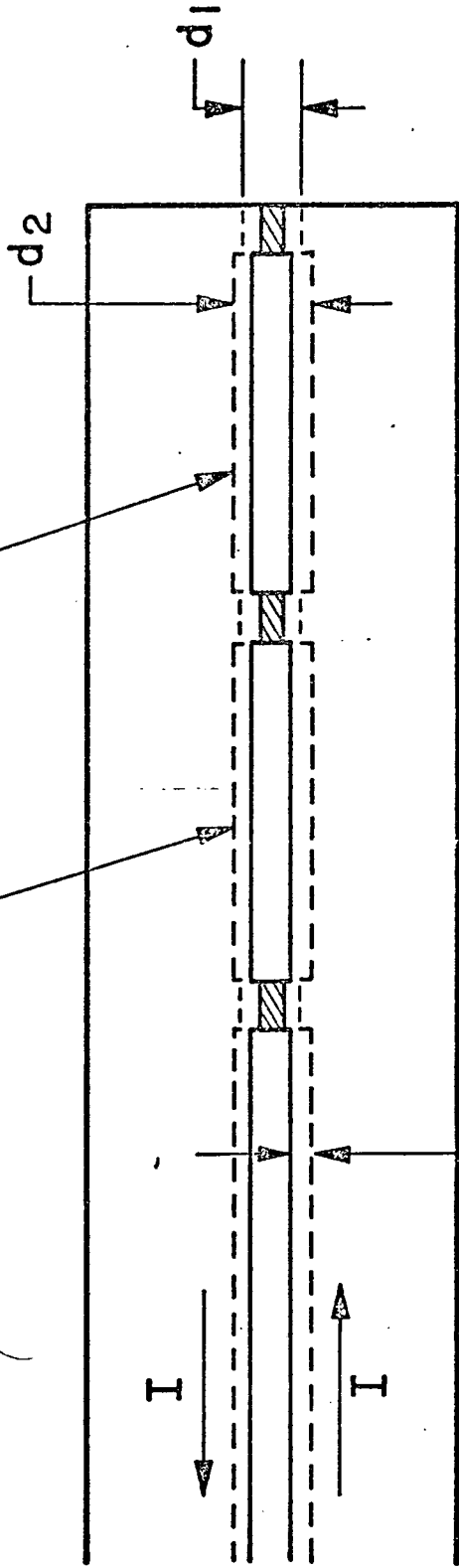
$$d) L_1 = .1\lambda_J, L_3-L_2 = .1\lambda_J, L-L_4 = .1\lambda_J, (L_2-L_1)d_2 = 20\lambda_J d_1,$$

$$(L_4-L_3)d_2 = 20\lambda_J d_1.$$

The dimensions are chosen for easy comparison of the interference patterns.

INTERFERENCE LOOP 1 AREA

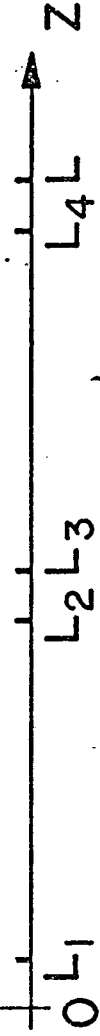
INTERFERENCE LOOP 2 AREA

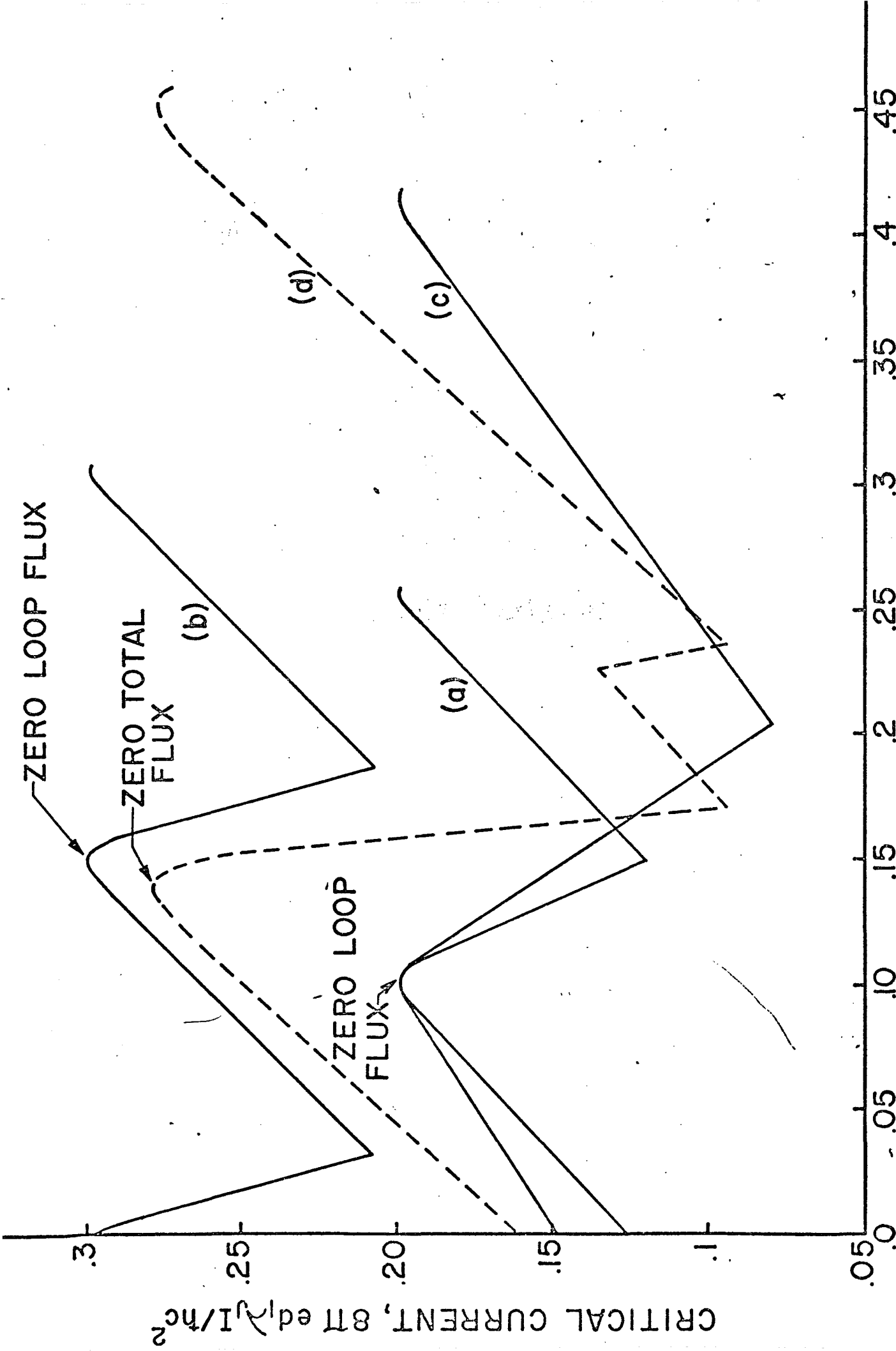


\otimes H_e

LONDON PENETRATION DEPTH

X





APPLIED MAGNETIC FIELD, $2ed_j \lambda_j H_e / hc$

CRITICAL CURRENT, $8\pi e d_j I_c / hc^2$

APPENDIX II

Flux Quantization in Josephson
Junction Quantum Interference Devices

By

D. L. Stuehm and C. W. Wilmsen

Physical Review Letters

FLUX QUANTIZATION IN JOSEPHSON JUNCTION QUANTUM INTERFERENCE DEVICES*

D. L. Stuehm and C. W. Wilmsen

Electrical Engineering Department

Colorado State University, Ft. Collins, Colorado

ABSTRACT

It is generally accepted that the peak values of the critical current through a Josephson junction quantum interference device are separated by multiples of the flux quantum $\phi_0 = hc/2e$. In this paper we show that for non-zero junction lengths, adjacent current peaks are separated by less than the flux quantum.

A quantum interference device is formed when two Josephson junctions are placed in a superconducting ring^{1,2} (see Fig. 1). In a simple superconducting ring without the junctions, the flux threading the non-superconducting area of the ring is quantized in order that the wavefunction of the super electrons be single valued. When the two Josephson junctions are placed in the ring, the flux is no longer quantized.³ The critical current through the quantum interference device is a periodic function of interference loop flux and it is generally believed¹⁻³ that the peaks of the critical current are separated by multiples of the flux quantum, $\phi_0 = hc/2e$. In this paper we show that if there is no spatial variation of the junction current, adjacent current peaks are separated by ϕ_0 . However, for non-zero length junctions, there exists a spatial variation of the junction currents and for this case we show that the adjacent current peaks are separated by less than ϕ_0 . These results

are especially important in the application of the interferometer to the measurement of magnetic fields.

We first consider the case of no spatial variation of the junction currents. The current density through a Josephson junction is related to the pair phase, $\phi(z)$, across the junction by

$$J(z) = j_1 \sin \phi(z). \quad (1)$$

For two equal junctions in parallel the total current density is

$$J = j_1 \sin \phi_1(z) + j_1 \sin \phi_2(z). \quad (2)$$

With no spatial variation of the phase in the junctions, $\phi_1(z) = \phi_1$ and $\phi_2(z) = \phi_2$. The peak value of the critical current occurs when $\phi_1 = \pi/2$ and $\phi_2 = \phi_1 + 2N\pi$, where $N = 0, 1, 2, 3, \dots$. The $2N\pi$ phase difference is due to the flux in the interference loop and occurs when $\Phi = N\Phi_0$. Thus the period of the interference pattern is Φ_0 for constant phase across the junctions.

However, the pair phase across a junction of finite size is not constant but is related to the local field by

$$\frac{d\phi(z)}{dz} = \frac{2ed}{\hbar c} H(z), \quad (3)$$

where $d = 2\lambda_L + T$, λ_L is the London penetration depth and T is the thickness of the insulator. For most cases $H(z)$ is positive⁴ i.e., the applied flux is greater than the induced flux, which implies that the phase increases

within the junction for positive z . This is true for both junctions in the quantum interference device.

With approximately one flux quantum in the interference loop, the critical current reaches a peak value as illustrated in Fig. 2a. At this peak the phase across the first junction starts at slightly less than $\pi/2$ and increases to more than $\pi/2$. The phase across the second junction starts at less than $5\pi/2$ and increases. This shows qualitatively that at peak critical current the phase between the junctions is less than 2π and therefore $\phi < \phi_0$. Increasing the flux in the interference loop until the phase difference between the junctions is 2π , as shown in Fig. 2b, causes the critical current to decrease. This decrease of the critical current with increasing flux is due to the reduction of the current in the first junction as shown by De Waele et al.³ and verified by our numerical calculations. For each succeeding peak value of critical current the phase change is larger because of the greater field. Therefore, the interference pattern is still periodic but the period is less than ϕ_0 .

To obtain a quantitative measure of the period of the interference pattern, we have numerically solved Eqs. 1, 2, 3, and Maxwell's equation

$$\frac{dH(z)}{dz} = \frac{4\pi}{c} J(z) \quad (4)$$

subject to boundary conditions similar to those of Owen and Scalapino⁵ to compute the pair phase $\phi(z)$ across the junctions and across the interference loop. These equations take into consideration the magnetic flux due to the applied magnetic field (H_e) and the flux due to the current in the superconducting links connecting the Josephson junctions, but neglect the flux due to

the mechanical momentum of the electrons. The spatial derivative of the pair phase (eq. 3) gives the magnetic field everywhere in the device, from which the flux in the interference loop can be calculated. The boundary conditions are a function of the critical current and the applied magnetic field. Integrating Eq. 2 over the spatial dimensions of both junctions provides a check on the applied critical current used in the boundary conditions. These calculations consider the spatial variation of the phase in the junctions and provide a plot of critical current as a function of applied flux.

The results of these numerical calculations are shown in Fig. 3 where the flux in the interference loop at the peak value of critical current is plotted versus the ratio interference loop area/junction area.⁶ Different sized junctions and interference loop areas were used to verify that Fig. 3 is independent of junction area (assuming equal permeabilities in the interference loop and in the junction). Fig. 3 shows that the flux quantization occurs only when the junction effects are negligible. This implies that with non-zero junction lengths, measurements of absolute magnetic fields by counting the interference peaks can be in error. The amount of error depends on the ratio of interference loop area/junction area and the number of peaks counted. For example, the calculation shows that with an interference loop area/junction area ratio of 400, the 192nd current peak occurs with an interference loop flux of $191.5 \phi_0$. This error may not be critical for many applications, but for measuring fields that are multiples of the flux quantum, major discrepancies between theory and experiment could be obtained.

The period of the interference pattern has been shown to be qualitatively and quantitatively less than the flux quantum. This is a direct result of taking into consideration the spatial dependence of the junction phase on the local H field. Numerical calculations show the results are valid for both

the symmetrical-feed and asymmetrical⁷-feed devices. The abscissa of Fig. 3 could also be labeled "Approximate ratio of junction period/interference loop period", or "approximate number of interference peaks in one junction period". With either of the above labels these results for junctions could possibly be extended to other methods of forming Josephson effect devices such as metal bridges, slugs and point contacts.

REFERENCES

* Supported in part by the National Aeronautics and Space Administration.

1. R. C. Jaklevic, J. Lambe, J. E. Mercereau, and A. H. Silver, Phys. Rev. 140, A1628 (1965).
2. J. E. Zimmerman and A. H. Silver, Phys. Rev. 141, 367 (1966).
3. A. Th. A. M. DeWaele and R. De Bruyn Ouboter, Physica 41, 225 (1969).
4. $H(z)$ is not positive in the first junction for the cases of zero interference loop flux and for the case of very large junctions with a large interference loop area. Our numerical calculations indicate that for large junctions with a large interference loop area, the period of the quantum interference pattern is also less than the flux quantum.
5. C. W. Owen and D. J. Scalapino, Phys. Rev. 164, 538 (1967).
6. Junction area is the area of the junction normal to the applied field, which is Ld where L is the length of the junction and d is the insulator thickness plus $2\lambda_L$.
7. J. Clarke and J. L. Paterson, Appl. Phys. Lett. (to be published); J. Clarke, Phys. Today Aug., 30 (1971).

FIGURES

Fig. 1. The geometry of the interference device. The shaded areas are the Josephson junctions. H_e is the applied magnetic field normal to the paper. I is the current per unit width through the device. I_1 and I_2 are the currents per unit width through junctions 1 and 2 respectively.

Fig. 2. Critical current density at two values of applied flux. Area I_1 is the current per unit width through junction 1 and area I_2 is the current per unit width through junction 2.

- a) Peak value of the critical current flows for less than one flux quantum in the interference loop.
- b) At one flux quantum in the interference loop, less than peak current flows through the device.

Fig. 3. Flux in the interference loop at the peak value of critical current versus the ratio interference loop area/junction area.

